Time-dependent knotting of agitated chains

Ingrid Gendron,[*] Katherine Savard,[*] Xavier Capaldi,[*] Zezhou Liu, Lili Zeng, and Walter Reisner[†]
Physics Department, McGill University, 3600 rue University, Montreal, Canada

Luc Capaldi
Department of Mechanical Engineering, University of Vermont, Burlington, Vermont 05405, USA

(Received 1 December 2020; accepted 19 February 2021; published 10 March 2021)

Agitated strings serve as macroscale models of spontaneous knotting, providing valuable insight into knotting dynamics at the microscale while allowing explicit analysis of the resulting knot topologies. We present an experimental setup for confined macroscale knot formation via tumbling along with a software interface to process complex knot data. Our setup allows characterization of knotting probability, knot complexity, and knot formation dynamics for knots with as many as 50 crossings. We find that the probability of knotting saturates below 80% within 100 s of the initiation of tumbling and that this saturation probability does not increase for chains above a critical length, an indication of nonequilibrium knot-formation conditions in our experiment. Despite the saturation in knot formation, we show that longer chains, while being more confined, will always tend to form knots of higher complexity since the free end can access a greater number of loops during tumbling.

DOI: 10.1103/PhysRevE.103.032501

Knots form at all length scales due to random motion of the free ends of a string or chain. Macroscale knotting usually manifests as tangled wires or snarled hair; in rare cases, knotting of the umbilical cord during fetal gestation can cause complications in pregnancy and childbirth [1]. On the microscale, polymer knots can have significant biological and technical implications. DNA is a long-chain polymer that can occur in linear or circular conformations. Complex knots have been observed on the DNA confined within the viral capsid of the P4 icosahedral bacteriophage [2]. Experimental studies show that these knots limit the rate at which viruses are able to eject their DNA into a target cell [3]. In *E. coli*, specialized topoisomerases are required to resolve knots in their genome which can inhibit cellular replication [4]. From a technological perspective, knots pose challenges for single molecule DNA analysis devices, e.g., based on nanopores and nanochannels. Knots inhibit translocation of long dsDNA molecules and block access to DNA contour stored in the knot region [5]. In addition knots are observed in proteins, and work to understand their formation and biological role has increased rapidly in recent years. However, protein knotting is vastly more complex than DNA knotting due to the variety of constituent amino acids and their interactions [6–8].

Chain compression via applied fields or confinement plays a crucial role in knot formation. Knot formation in viral systems is attributed to the very high dsDNA confinement in the capsid [2]. Simulations of simple knotted proteins confined in chaperonin cages show that confinement increases both knotting probability as well as the rate of protein folding [9,10]. Spontaneous knotting of single dsDNA molecules has been explored with assays designed to induce controlled compression in single molecules. In one approach, DNA compression is induced in high electric fields [11–14]. In a second approach, the nanofluidic knot factory, compression is induced by using hydrodynamic flow to compress single molecules against a barrier in a nanochannel [15,16]. Yet, while these methods produce complex knots in DNA, the diffraction limit precludes a more in depth study of knot topology with fluorescence microscopy.

While chain compression plays a key role in enhancing knot formation, these studies highlight the essential role played by microscopic fluctuations in driving knot-formation kinetics. In particular, knots do not appear to form instantaneously after compression. Amin *et al.* [15] identified a minimum waiting time for which the molecule must be held in a compressed state for knotting probability to become appreciable. In order for knots to form, there must also exist a feasible kinetic pathway for the chain free end to pass through an existing loop. In particular, in the electric field driven compression process, flows induced by an electrohydrodynamic instability may lead to a nonequilibrium tumbling motion that might promote favorable kinetics [12]. While a tumbling motion is unlikely in the knot factory due to the ultralow Reynolds number hydrodynamics, Brownian fluctuations may provide the necessary local agitation to drive knot formation [15]. A fascinating open question is to what degree knot formation may differ between equilibrium and nonequilibrium knot-generating processes.

Macroscopic systems featuring agitated strings can provide detailed insight into knot topology and knot-formation mechanisms. Early macroscopic knotting systems used vibrating plates [17,18] or driven hanging chains [19]. More recently, Raymer *et al.* [20] used a rotating box to characterize knotting probability and knot complexity as a function of chain length. They found that knotting probability rises rapidly with string length but saturates at less than 60% for strings above a critical

[*]These authors contributed equally to this work.
[†]reisner@physics.mcgill.ca

length (equal to around 2 m for their study). They observed a similar trend in knot complexity. The saturation phenomenon was attributed to wedging of the string inside the box, with the suggestion that a more flexible string tumbled for a longer time would eventually approach 100% knotting probability, as is theoretically expected. This work was extended to circular chains in a rotating sphere by Soh *et al.* in 2019 [21]. Both studies primarily measured the effects of increasing string contour length at fixed agitation time. The majority of knots were formed after only agitating for 10 s (10 revolutions for Raymer *et al.* and 36 revolutions for Soh *et al.*) and had a relatively simple topology (crossing number less than 12). Both studies observed the saturation in knotting probability and complexity as string length was increased.

Here we use a macroscopic rotating box setup to explore the time dependence of knot formation on single tumbled strings. In contrast to previous work that focused on the dependence of knotting probability on string length [20,21], here we focus on how knotting probability and topological complexity vary with agitation time. Knotting probability is observed to grow and then reach a saturating knotting probability, as observed in nanochannel compression experiments [15]. Surprisingly, we observe that, even for very long agitation times, the knotting probability of long strings does not approach 100%. We propose that this effect is a property of nonequilibrium knot formation and outline the key differences between equilibrium and nonequilibrium cases and how they can be applied to understand knot formation in biological systems. In addition, using a custom software package, we characterize knots with crossing numbers as high as 50—a knot complexity similar to that found in viral capsids [2]. This capability enables us to track the time evolution of the full knot complexity distribution. We find that the distribution of knot complexity evolves from a peak at trefoil knots at lower times to a distribution where knots of a wide range of complexity are equally probable.

I. EXPERIMENTAL METHOD

A. Physical setup

The physical setup consists of an acrylic cubic box measuring 0.15 m on each axis. The box is rotated by a stepper motor (Nema 17, model 17HS19-2004S1) with an external power supply controlled by an Arduino UNO and an Adafruit motor shield. Angular velocity and agitation time are controlled via serial communication between a PC and the Arduino UNO.

B. String preparation

For our model chain, we used a string with a polyester strand core and a braided nylon cover designed to resist stretching (McMaster-Carr 3696T16). The string had a diameter of 3.2 mm and a linear density of 0.05 g/cm. The cut ends were melted to avoid fraying during the experiment. Each sample was tumbled for 20 min before data collection to eliminate residual coil structure from packing and shipping. Flexural rigidity was estimated with the Euler small displacement formula by extending the free end of the string off the edge of a surface and measuring its deflection under its own weight. We found an average flexural rigidity of 1.06×10^3 dyn cm^2.

C. Experimental protocol

We begin the experiment by positioning the box so that its opening is oriented directly upwards. We then manually feed the string into the box center, creating a quasirandom initial configuration [Fig. 1(a)]. The box is subsequently sealed and tumbled with an angular velocity of 1 revolution per second for a specified time duration ranging from 5 to 420 s [Fig. 1(b)]. This particular angular velocity is selected so that the string is able to tumble over itself during rotation (too high a rotation speed causes the string to remain pressed against the box surface with very little mobility). Raymer *et al.* also observed this decrease in tumbling motion at higher rotational speeds [20]. After agitation [Fig. 1(c)], each end of the string is grasped from above and pulled directly upward. As we ensure that the chain ends are not pulled though any loops when the chain is lifted, there will be no disturbance to the two-dimensional (2D) projection. Since a knot is mathematically defined as a closed loop, we treat the two ends as joined and manually manipulate the knot to ensure all crossings are clearly visible before photographing [Fig. 1(d)]. The knot is then removed and the entire process repeated a minimum of 50 times for any given combination of chain length and agitation time.

To verify that our extraction procedure and initial conditions were not leading to further knotting, we performed a set of trials with no agitation; the string was only introduced into the box and then removed. This never resulted in nontrivial knots, verifying that the observed knotting occurred exclusively due to the tumbling.

D. Topological analysis

Knot topological complexity is characterized by a quantity known as the minimum strand crossing number (n_c). Crossings are found by taking the 2D projection of a knot and finding any point at which two strands cross each other. While it is easy to count the number of crossings in a given knot, many of these crossings are not fundamental to determining the knot topology. Reidemeister proved in 1927 that two identical knots can be related by any combination of three topological moves: twist, poke, and slide [23]. Since these moves cannot fundamentally modify the knot, they can be used to simplify the raw experimental knot configurations with the goal of reaching the minimum crossing number describing the given knot's topological complexity. This process can be performed by hand for simple knots but our results contain knots with very high crossing numbers that are too complex to simplify by hand (e.g., knots with 75 crossings that can be simplified to 50 fundamental crossings). We perform this simplification process computationally with the Pyknotid module developed as part of the Scientific Properties of Complex Knots (SPOCK) project [24]. Given a set of three-dimensional (3D) coordinates describing the knot structure, this module can convert them to a 2D knot diagram and perform iterative Reidemeister moves to find the minimum crossing number. We developed our own custom

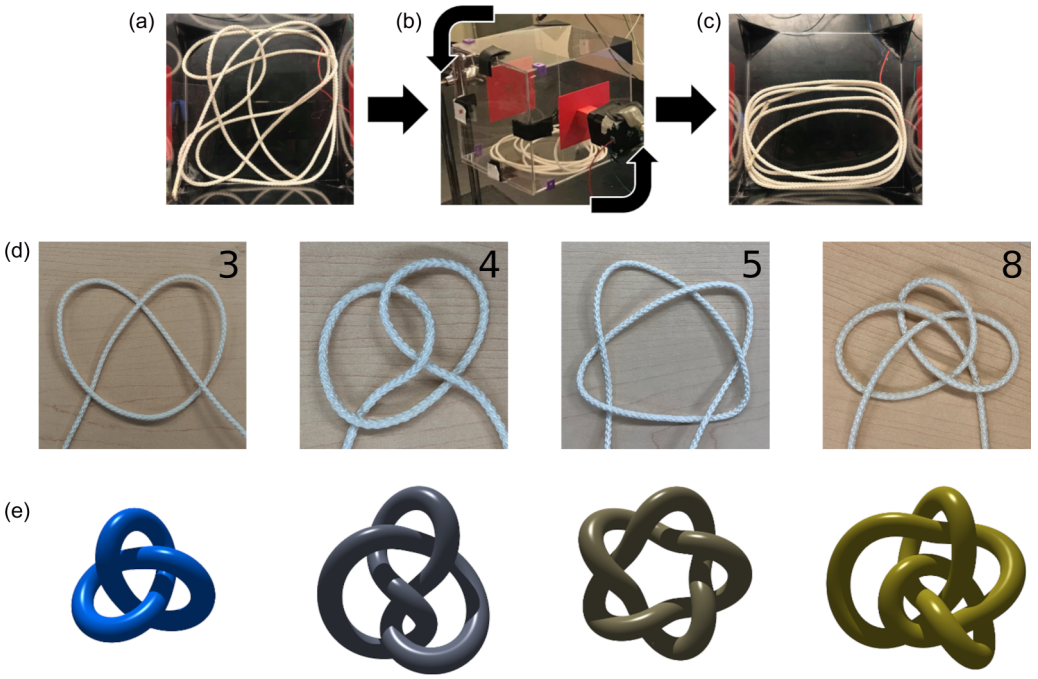

FIG. 1. Knot tumbling device and sample of knots formed. (a) Initial pseudorandom chain conformation after threading the chain into the box. (b) The box is sealed for agitation. (c) Resulting chain conformation after agitation. (d) Example knots formed during tumbling (labeled with their minimum number of strand crossings) and (e) their identified topology rendered in three dimensions with the Persistence of Vision Raytracer. Images of more complex knots can be found in the Supplemental Material [22].

software package to facilitate translation of raw knot images into the necessary 3D coordinates for input into Pyknotid [25]. Each experimentally obtained knot configuration, using photographs as a reference, was drawn in the software as a 2D projection with strand intersections clearly demarcated as overcrossings or undercrossings. The software then expressed these annotated 2D data as a set of 3D coordinates that were passed to the Pyknotid knot analysis back end. In general, we were able to process knots with crossing numbers as high as 50, of similar complexity to those found in viral capsids [2].

II. RESULTS AND DISCUSSION

A. Time evolution of knotting probability

The probability of knot formation as a function of agitation time is presented in Fig. 2 for various chain lengths. Each point is the average of approximately 50 knotting trials. At short agitation times, the probability of knot formation rises rapidly which was also observed by Raymer *et al.* [20]. However, our maximum agitation time is 1400% longer than that of Raymer *et al.* and we find the knotting probability saturates at a limiting probability (α) less than unity. We fit our results to an exponential function: $P_f = \alpha(-\exp(-t/\tau) + 1)$ where α is the saturation probability and τ is the time constant. Figure 3 gives the value of α as a function of chain length. The saturating knotting probability does not increase beyond the critical value observed for the 2-m string even after long periods of agitation (420 s).

Critically, these results disagree with predictions for equilibrium knotting. Knots form in equilibrium conditions when the free end of a chain undergoes a random walk. For an infinitely flexible coil, as the number of steps taken in the random walk tends to infinity, the probability of forming a nontrivial knot tends exponentially to unity [26]. Given a chain that is not infinitely flexible, computational studies suggest that the probability of forming a nontrivial knot, P, is related to the contour and characteristic lengths (N and N_0, respectively) via $P = 1 - \exp(-N/N_0)$ [27,28]. The characteristic length, N_0, is set by our box confinement and string properties, which were not varied. The contour length, N, was varied by increasing the length of string introduced into the box. Note that, as there was no corresponding increase in knotting probability with increased contour length beyond 2 m, our results disagree with this relationship. One possible explanation for the observed saturation is limited chain mobility arising from volume exclusion in tight confinement [29]. This was observed experimentally by Raymer *et al.* [20], who noted that increasing confinement induces wedging of the string in the box, reducing the tumbling motion which normally favors knot formation. However, we are confident that we are not yet in the wedging regime, as all chain lengths used in our setup were able to tumble freely throughout the entire duration of agitation.

B. Time evolution of knot complexity

Figure 4 presents the mean minimum crossing number ($\langle n_c \rangle$) of observed knots as a function of agitation time. Increased agitation time elevates $\langle n_c \rangle$ but after sufficiently long agitation, a limiting $\langle n_c \rangle$ value is reached. Note that the saturating $\langle n_c \rangle$ value, in contrast to the behavior observed for knotting probability, does not saturate with increasing string length, but increases monotonically (Fig. 4 compared to Figs. 2 and 3). While the maximum measured knotting

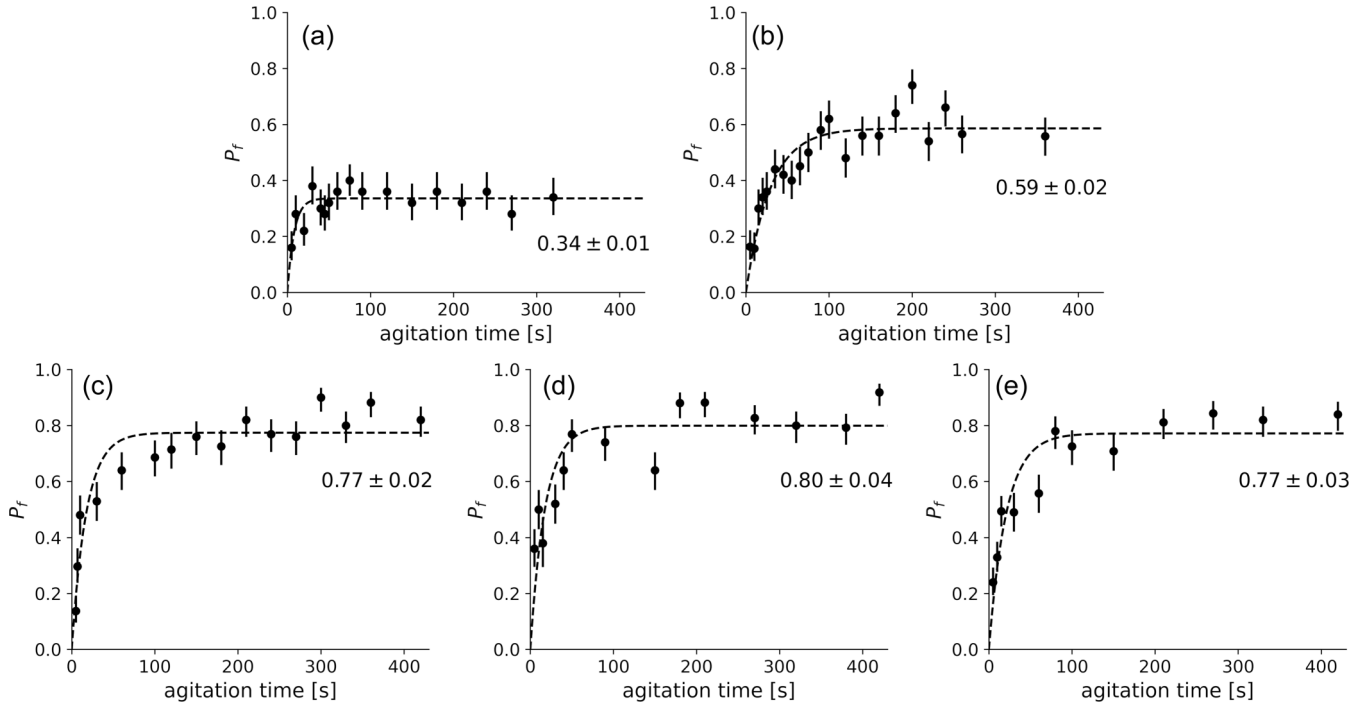

FIG. 2. Measured probability of forming a knot versus agitation time. Error bars correspond to standard error determined with a Wilson binomial proportion confidence interval. The line is a nonlinear least-squares fit to an exponential function $P_f = \alpha(-\exp(-t/\tau) + 1)$ where α is saturation probability. Text annotation shows the saturation probability (α). (a) 0.75-m string, (b) 1-m string, (c) 2-m string, (d) 3-m string, and (e) 6-m string.

probabilities for 2- and 3-m strings were in agreement, the longer chain still produced more complex knots. Raymer *et al.* propose a simplified knotting model that suggests the confined string will always form loops with which a free end can interact. They posit that $\langle n_c \rangle$ should saturate above some limiting number of confined loops [20]. In their experimental and simulation results, that limit was expressed around three to four loops. Our string, which is not infinitely flexible, also tended to form loops as it tumbled. The coil conformation was intermediate between two states: a circle with diameter equal to the box width and a square whose dimensions closely followed those of the box. Given the geometry of the confinement, $(0.15\ \text{m})^3$, we can assume each loop occupies between 0.47 and 0.6 m of the total string length. Thus the 2- and 3-m strings have four and six loops, respectively. Given prior results, we expect $\langle n_c \rangle$ to saturate at the 2-m string length but we do not observe this saturation so it is clear that other factors play a role.

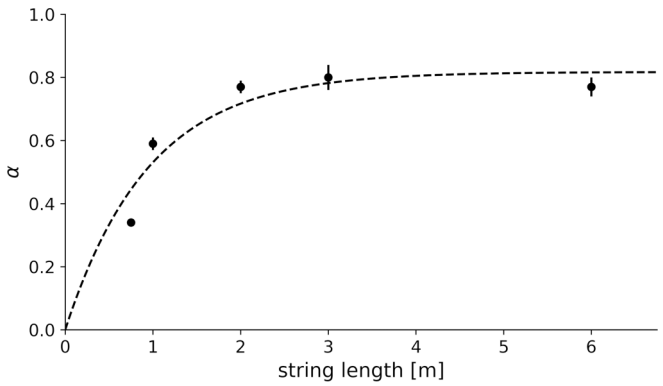

FIG. 3. Saturating knotting probability as a function of string length. Error bars correspond to uncertainty in fits presented in Fig. 2. The line is a nonlinear least-squares fit to an exponential function.

To explore this point further, we can investigate the time evolution of the knot complexity distribution. Figure 5 gives the probability of forming a knot of a specific crossing number for four agitation time intervals. The data were grouped so that data sets with similar $\langle n_c \rangle$ values are grouped into larger time intervals, providing us with snapshots of the distribution in knot topology for different time ranges. Each individual subplot represents data from 100–200 knots. The division into groups is shown in Fig. 4(d). At short agitation times [Fig. 5(a)], there is a strong peak centered at $n_c = 3$ and the highest complexity we observe is a knot with $n_c = 16$. As the agitation time is increased, the crossing number distribution flattens. At long agitation times [Fig. 5(d)], there is no noticeable peak and the formation of knots between crossing numbers 4 to 20 are approximately equiprobable. This result suggests that simple knots are formed first and then through further agitation they evolve into more complex knots. In contrast to our results, measurements of knot complexity in viral capsids reveal a peak centered around the 25–30 crossing range with only a small percentage of knots with low complexity [2].

C. Distribution of knot complexity

The probability of forming a knot of a certain crossing number is plotted in log-linear space for the three increasing

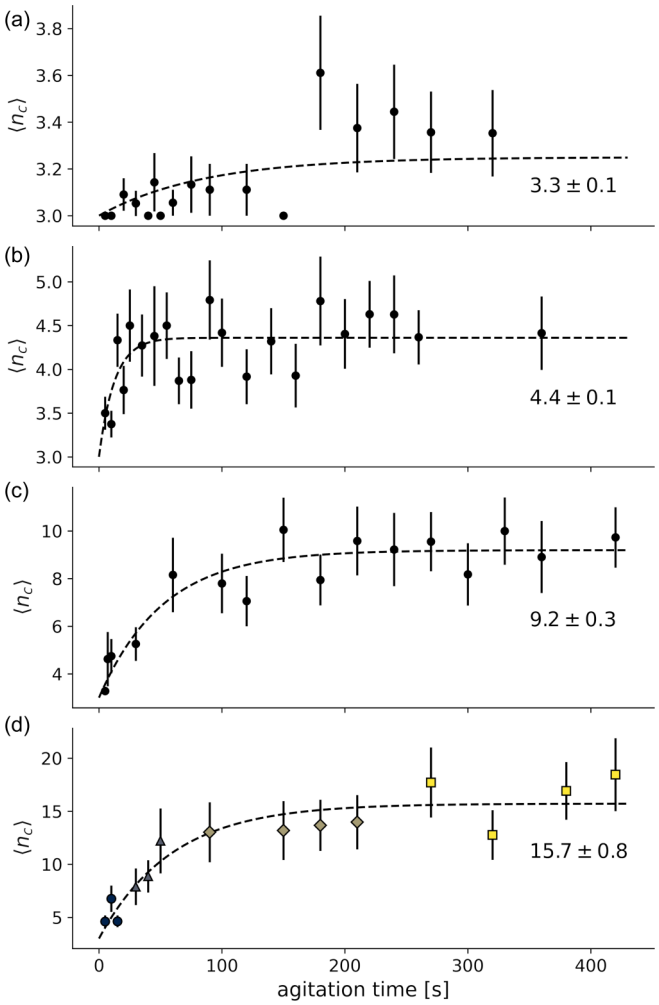

FIG. 4. $\langle n_c \rangle$ as a function of agitation time for different lengths of string (omitting trivial knots). Error bars correspond to standard error. The line is a nonlinear least-squares fit to an exponential function $\langle n_c \rangle = \alpha(-\exp(-t/\tau) + 1)$ where α is the saturation limit and τ is the time constant. (a) 0.75-m string with $\alpha = 3.3 \pm 0.1$, (b) 1-m string with $\alpha = 4.4 \pm 0.1$, (c) 2-m string with $\alpha = 9.2 \pm 0.3$, and (d) 3-m string with $\alpha = 15.7 \pm 0.8$. Different shapes are used to represent grouping used in Fig. 5: circles (5–15 s), triangles (30–50 s), diamonds (90–220 s), and squares (270–420 s).

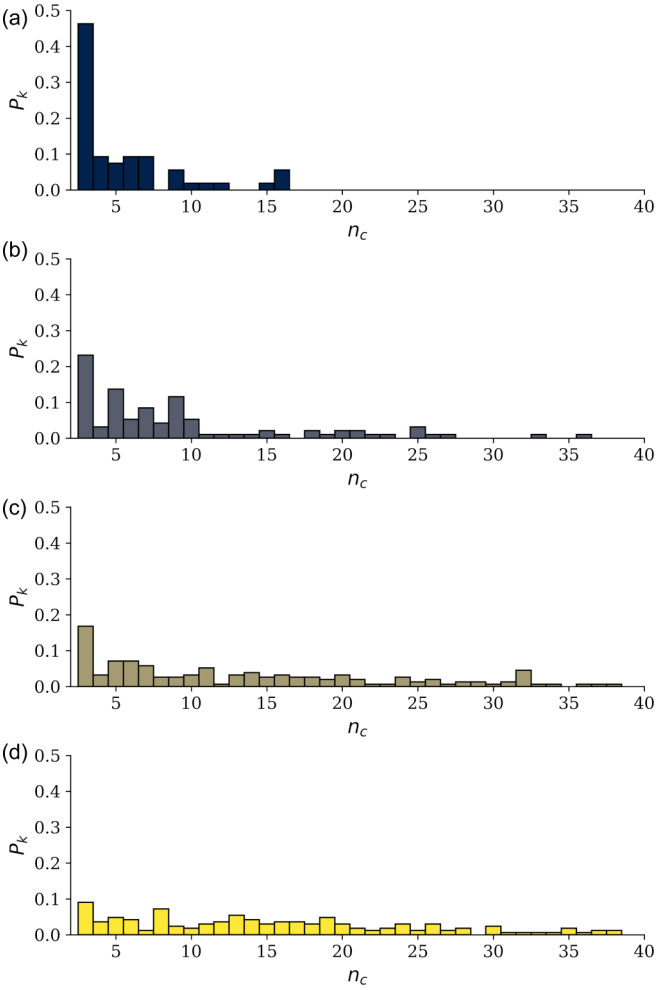

FIG. 5. Probability of forming a knot of a given crossing number for a 3-m string, at agitation time intervals (a) 5–15 s, (b) 30–50 s, (c) 90–220 s, and (d) 270–420 s. Each time interval groups data from multiple agitation times, such that data with similar crossing numbers are represented in one subplot.

lengths of string in Fig. 6. Random walk models predict that the probability of forming any given knot decreases exponentially with increasing crossing number [30]. In contrast to the predicted behavior [30], only knots with odd crossing number (solid circles in Fig. 6) exhibit exponential decay whereas a subset of the even-crossing-number knots (open circles) increase in formation probability with increasing crossing number. These separate trends break down after ten crossings. No existing models explain this behavior. Raymer *et al.* presented their results in a similar figure where a distinction between odd- and even-crossing knots can be observed but to a lesser extent. In particular, while they do not observe that a subset of their even-crossing knots increases in formation probability, like we observe, a subset of their even-crossing knots appears to decrease in formation probability at a slower rate [20].

The probability of forming a low complexity knot of a given crossing number may be highly dependent on the string's initial configuration. Figure 7 shows a simplified schematic of two possible starting string configurations. Depending upon the initial configuration of the coil (containing only two loops in this case), the free end can make a single move and form one of two simple knots with even or odd crossings. If the free end of the chain is more likely to pass beneath both strands in Fig. 7(b), that would explain the higher probability of forming more complex even-crossing knots. In addition, this would suggest that any knot with crossing number satisfying the following condition (where n_{loop} is the number of loops) will not follow this trend: $n_c > 2(n_{\text{loop}} + 1)$. Such knots require more than a simple move over or under a given number of loops to form. This behavior can be seen quite clearly in Fig. 6. It is not clear from the experiment why the terminal end would be more likely to pass inside multiple loops when the coils are twisted. In addition, it is unclear why the eight-crossing knot is more probable for the 1-m string [Fig. 6(b)] when it should only have one or two loops. This

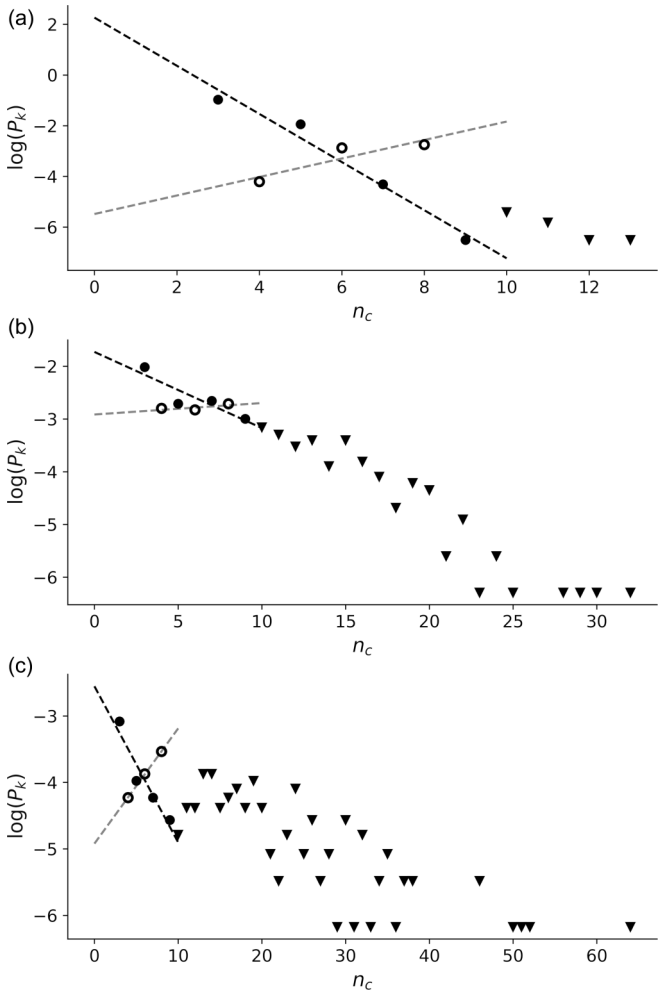

FIG. 6. Log-linear plot of probability of forming a knot of a certain crossing number: (a) 1 m, (b) 2 m, and (c) 3 m. Open circles indicate even-crossing-number knots, solid circles indicate odd-crossing-number knots, and triangles are used for knots above ten crossing number irrespective of their parity. Trends for odd- and even-crossing-number knots (with under ten crossings) are fitted to separate linear regressions.

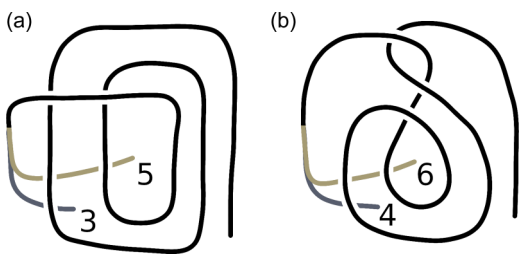

FIG. 7. Schematic of two potential coil configurations before knotting. (a) A typical string configuration. If a free end of the chain passes under the outer loop, a knot with three crossings will form. If it passes under both loops a knot with five crossings will form. (b) A twisted coil configuration. If a free end of the chain passes under the outer loop a knot with four crossings will form. If it passes under both loops a knot with six crossings will form.

TABLE I. Approximate percentage of composite knots formed for strings of various lengths.

Length (m)	Composite knots	Total knots	%
0.75	0	280	0.00
1.0	2	671	0.30
2.0	18	541	3.33
3.0	19	480	3.96
6.0	50	417	11.99

behavior should break down after the six-crossing knot based upon our hypothesis. Further experimental work is necessary to clarify this behavior.

D. Composite knot formation

Although we focus on the formation of prime or indecomposable knots given their statistical dominance, we were able to observe supplementary trends in the formation of composite knots which are composed of multiple prime knots formed on a single strand. Table I shows the emergence of composite knots in the overall data at increasing string lengths, represented as both the number of composite knots observed and their percentage with respect to the total number of knots formed. Clearly composite knots become more probable with increasing string length. This is in agreement with simulation work that has shown increased contour length for a fixed confinement volume, and thus increased effective confinement, leads to a higher proportion of composite knots [29]. Interestingly, there was no observed correlation between agitation time and composite knot formation. It was also clear that the majority of these composite knots were formed at both ends of the string. In other words, each of the two free ends performed the necessary braid moves to form a knot, each of which was completely distinct from that formed at the other end.

E. Nonequilibrium knotting

Theoretical work on knot formation uses equilibrium conditions where knotting is primarily driven by strand crossings by nonexcluding volume chains. This should be equivalent to the Brownian motion of the free end of the chain but is more computationally efficient. For the confined and unconfined cases, knotting probability approaches unity as contour length increases [2,26,29,31]. However, for strings longer than 2 m, we find the probability saturates below 80%. This saturation has been observed in macroscale knotting experiments since Hickford *et al.* measured knotting probability below 40% in a chain on a vibrating plate [18]. Subsequent papers on macroscale knot formation also observed the knotting probability to saturate below 100% [20,21]. At the microscale, results differ from theoretical work as well: mature viruses only exhibit 47% knotting [2]. We propose that this is the result of fundamental differences in equilibrium versus nonequilibrium knotting.

Measured knotting probabilities result from a contest between knotting and unknotting rates which are limited by the motion of the chain free end. In an equilibrium system, the

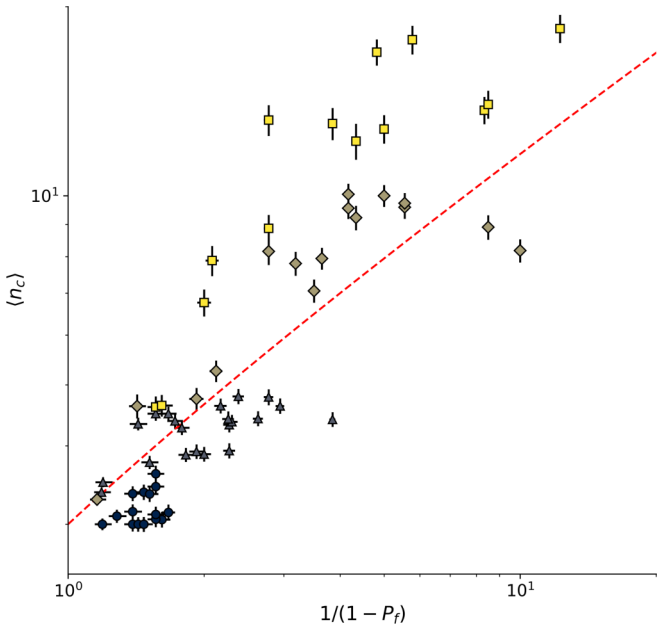

FIG. 8. Log-log plot of $\langle n_c \rangle$ as a function of $1/(1-P_f)$. Vertical error bars correspond to standard error in $\langle n_c \rangle$. Horizontal error bars correspond to standard error determined with a Wilson binomial proportion confidence interval. The line is from the empirical formula for universal knotting proposed by Dai *et al.* [32]: $\langle n_c \rangle = 4/\sqrt{1-P_f} - 1$. Different shapes are used to represent different string lengths: circles (0.75 m), triangles (1 m), diamonds (2 m), and squares (3 m).

end can freely interact with the full chain contour resulting in knots that are not localized to a particular region. For example, in the nanofluidic knot factory, knots were observed inside the chain and then diffused to the ends [15]. Recently Sharma *et al.* studied equilibrium knots directly using large diameter nanopores (20 nm). They found knotting probabilities and distribution of knot types that agreed well with simulations of equilibrium knotting. In particular, they confirmed that equilibrium knots form with uniform probability along the length of the chain [5]. In contrast, we propose that our and other macroscopic knot-formation systems operate in a nonequilibrium regime fundamentally limited by the motion of the chain ends relative to adjacent loops. In this regime, knots are typically formed near the chain ends as the end has limited mobility relative to its mobility in equilibrium conditions. For example, during tumbling the chain tends to form a coil and only the segment ranging from the end to the sharp corner of the coil is capable of crossing over and under adjacent strands to form knots. The unknotting rate is high because, when knots are localized near the end of the chain, they are easily undone by subsequent agitation [18]. The balance between knotting and relatively high unknotting rates results in knot formation probabilities below unity in nonequilibrium systems.

Dai *et al.* proposed a universal relationship between $\langle n_c \rangle$ and P_f for equilibrium knotting [32]: $\langle n_c \rangle = 4/\sqrt{1-P_f} - 1$. This relationship is completely independent of chain length, stiffness, and confinement. Prior simulation work [29] and experimental results from viral mutant DNA [2] fit the relationship well. As can be seen in Fig. 8, our results are significantly offset from the theoretical trend for equilibrium knotting. In addition, chains of varying length, sharing the same knotting probability, exhibit different $\langle n_c \rangle$. These discrepancies reinforce the fact that our experimental system is nonequilibrium.

Differences in behavior between equilibrium and nonequilibrium knotting has implications for biological systems. For example, mature viruses only exhibit 47% knotting relative to mutants which exhibit 95% knotting [2], suggesting that there is some internal packing mechanism to reduce the rate of knot formation as a purely equilibrium system should trend toward 100% knotting as observed in the mutant. Indeed, studies of the packaging motors employed by viruses show that they exert significant forces (>60 pN) to spool DNA tightly within the capsid, giving rise to a nonequilibrium packing [33].

III. CONCLUSION

In this work, we studied the spontaneous formation of knots along agitated linear chains. We found that knotting probability saturates below 100% even for longer strings but the complexity of knots formed still increases with increasing chain length. By studying the time evolution of the knot complexity distribution, we show that simple knots will form first before evolving into more complex knots. With our long-time agitation study, we are finally able to probe macroscale knots of a similar complexity to those found in viral capsids [2]. Raymer *et al.* investigated the effects of varying string flexibility, agitation rate, and confinement geometry but work is necessary to explore these parameters further and to probe their effects on the saturation level of knotting probability. In particular, Raymer *et al.* observed that knotting probability increased for higher string flexibility [20]. In addition, it is not yet clear how the method of agitation influences knot formation (e.g., uniform tumbling in one direction versus tumbling where the axis of rotation is not fixed and can change during rotation). Future experiments could use a simplified version of nonuniform tumbling by simply changing the direction of rotation along one axis during agitation.

ACKNOWLEDGMENTS

This work was funded with support from the National Sciences and Engineering Research Council of Canada (NSERC), Discovery Grant No. RGPIN-2018-06125. We thank the staff of the McGill Physics 3D Lab, particularly Robert Turner and Harrisonn Griffin who assisted with the 3D printing and assembly of our experimental setup. We thank Saverio Biunno and Philippe Movafegh from whom we borrowed equipment from the pedagogical physics laboratories. We also thank Juan Yao (Justin) Li for helpful discussions and reviewing this manuscript.

[1] M. E. Szczepanik and A. C. Wittich, True knot of the umbilical cord: A report of 13 cases, Mil. Med. **172**, 892 (2007).

[2] J. Arsuaga, M. Vazquez, S. Trigueros, D. W. Sumners, and J. Roca, Knotting probability of DNA molecules confined in

restricted volumes: DNA knotting in phage capsids, Proc. Natl. Acad. Sci. USA **99**, 5373 (2002).
[3] N. C. H. Lim and S. E. Jackson, Molecular knots in biology and chemistry, J. Phys.: Condens. Matter **27**, 354101 (2015).
[4] J. M. Sogo, A. Stasiak, M. L. Martínez-Robles, D. B. Krimer, P. Hernández, and J. B. Schvartzman, Formation of knots in partially replicated DNA molecules, J. Mol. Biol. **286**, 637 (1999).
[5] R. Kumar Sharma, I. Agrawal, L. Dai, P. S. Doyle, and S. Garaj, Complex DNA knots detected with a nanopore sensor, Nat. Commun. **10**, 1 (2019).
[6] D. Meluzzi, D. E. Smith, and G. Arya, Biophysics of knotting, Annu. Rev. Biophys. **39**, 349 (2010).
[7] P. F. Faísca, Knotted proteins: A tangled tale of structural biology, Comput. Struct. Biotechnol. J. **13**, 459 (2015).
[8] A. Nunes and P. Faísca, Knotted proteins: Tie etiquette in structural biology, *Topology and Geometry of Biopolymers* (American Mathematical Society, Providence, 2020), pp. 155–184.
[9] M. A. Soler, A. Rey, and P. F. N. Faísca, Steric confinement and enhanced local flexibility assist knotting in simple models of protein folding, Phys. Chem. Chem. Phys. **18**, 26391 (2016).
[10] J. Especial, A. Nunes, A. Rey, and P. F. Faísca, Hydrophobic confinement modulates thermal stability and assists knotting in the folding of tangled proteins, Phys. Chem. Chem. Phys. **21**, 11764 (2019).
[11] A. R. Klotz, B. W. Soh, and P. S. Doyle, Motion of Knots in DNA Stretched by Elongational Fields, Phys. Rev. Lett. **120**, 188003 (2018).
[12] J. Tang, N. Du, and P. S. Doyle, Compression and self-entanglement of single DNA molecules under uniform electric field, Proc. Natl. Acad. Sci. USA **108**, 16153 (2011).
[13] A. R. Klotz, V. Narsimhan, B. W. Soh, and P. S. Doyle, Dynamics of DNA knots during chain relaxation, Macromolecules **50**, 4074 (2017).
[14] V. Narsimhan, A. R. Klotz, and P. S. Doyle, Steady-state and transient behavior of knotted chains in extensional fields, ACS Macro Lett. **6**, 1285 (2017).
[15] S. Amin, A. Khorshid, L. Zeng, P. Zimny, and W. Reisner, A nanofluidic knot factory based on compression of single DNA in nanochannels, Nat. Commun. **9**, 1 (2018).
[16] Z. Ma and K. D. Dorfman, Diffusion of knots along DNA confined in nanochannels, Macromolecules **53**, 6461 (2020).
[17] E. Ben-Naim, Z. A. Daya, P. Vorobieff, and R. E. Ecke, Knots and Random Walks in Vibrated Granular Chains, Phys. Rev. Lett. **86**, 1414 (2001).
[18] J. Hickford, R. Jones, S. C. du Pont, and J. Eggers, Knotting probability of a shaken ball-chain, Phys. Rev. E **74**, 052101 (2006).
[19] A. Belmonte, M. J. Shelley, S. T. Eldakar, and C. H. Wiggins, Dynamic Patterns and Self-Knotting of a Driven Hanging Chain, Phys. Rev. Lett. **87**, 114301 (2001).
[20] D. M. Raymer and D. E. Smith, Spontaneous knotting of an agitated string, Proc. Natl. Acad. Sci. USA **104**, 16432 (2007).
[21] B. W. Soh, I. R. Gengaro, A. R. Klotz, and P. S. Doyle, Self-entanglement of a tumbled circular chain, Phys. Rev. Research **1**, 033194 (2019).
[22] See Supplemental Material at http://link.aps.org/supplemental/10.1103/PhysRevE.103.032501 for images of complex knots and a video of the knot formation process.
[23] K. Reidemeister, Elementare begrndung der knotentheorie, Abh. Math. Seminar Univ. Hamburg **5**, 24 (1927).
[24] A. J. Taylor and other SPOCK contributors, pyknotid knot identification toolkit, https://github.com/SPOCKnots/pyknotid, 2017.
[25] X. Capaldi and L. Capaldi, whyknot tkinter-based interface to pyknotid, https://github.com/xcapaldi/whyknot, 2019.
[26] D. W. Sumners and S. G. Whittington, Knots in self-avoiding walks, J. Phys. A: Math. Gen. **21**, 1689 (1988).
[27] K. Koniaris and M. Muthukumar, Knottedness in Ring Polymers, Phys. Rev. Lett. **66**, 2211 (1991).
[28] K. Koniaris and M. Muthukumar, Self-entanglement in ring polymers, J. Chem. Phys. **95**, 2873 (1991).
[29] C. Micheletti, D. Marenduzzo, E. Orlandini, and D. W. Summers, Knotting of random ring polymers in confined spaces, J. Chem. Phys. **124**, 064903 (2006).
[30] M. K. Shimamura and T. Deguchi, Knot complexity and the probability of random knotting, Phys. Rev. E **66**, 040801(R) (2002).
[31] E. J. J. van Rensburg, D. A. W. Sumners, E. Wasserman, and S. G. Whittington, Entanglement complexity of self-avoiding walks, J. Phys. A: Math. Gen. **25**, 6557 (1992).
[32] L. Dai and P. S. Doyle, Universal knot spectra for confined polymers, Macromolecules **51**, 6327 (2018).
[33] D. E. Smith, Single-molecule studies of viral DNA packaging, Curr. Opin. Virol. **1**, 134 (2011).